Geomechanics and Engineering, *Vol. 19, No. 2 (2019) 115-126*
DOI: https://doi.org/10.12989/gae.2019.19.2.115

Field test of the long-term settlement for the post-grouted pile in the deep-thick soft soil

Jin-Feng Zou, Tao Yang* and Dong-ping Deng

School of Civil Engineering, Central South University, No.22, Shaoshan South Road,
Central South University Railway Campus, Changsha, Hunan Province, People's Republic of China

(Received July 6, 2019, Revised September 23, 2019, Accepted September 26, 2019)

Abstract. The long-term settlement characteristics for the cast-in-place bored pile in the deep-thick soft soil are investigated by post-grouting field tests. Six cast-in-place bored engineering piles and three cast-in-place bored test piles are installed to study the long-term settlement characteristics. Three post-grouting methods (i.e., post-tip-grouting, post-side-grouting, and tip and side post-grouting) are designed and carried out by field tests. Results of the local test show that decreased settlements for the post-side-grouted pile, the post-tip-grouted pile and the tip and side post-grouted pile are 22.2%~25.8%, 30.10%~35.98% and 32.40%~35.50%, respectively, compared with non-grouted piles. The side friction resistance for non-grouted piles, post-side-grouted pile, post-tip-grouted pile and the tip and side post-grouted pile undertakes 89.6~91.3%, 94.6%, 92.4%~93.0%, 95.7% of the total loading, respectively. At last, the parameters back analysis method and numerical calculation are adopted to predict the long-term settlement characteristics of the cast-in-place bored pile in the deep-thick soft soil. Determined Bulk modulus (K) and a creep parameter (K_s) are used for the back analysis of the long-term settlement of the post-grouted pile. The settlement difference between the back analysis and the measurement data is about 1.11%-7.41%. Long-term settlement of the post-grouted piles are predicted by the back analysis method, and the predicted results show that the settlement of the post-grouted pile are less than 6 mm and will be stable in 30 days.

Keywords: post-grouting local test; long-term settlement; deep-thick soft soil; cast-in-place bored pile; back analysis method

1. Introduction

Deep soft soil foundation reinforcement is an inevitable part of pile foundation engineering, and the post-grouting technique is one of the most effective methods for foundation treatment. The post-grouting technique of pile is to inject the cement slurry into the base of the pile using the high-pressure pump to improve the bearing capacity, recover the bearing capacity of the ground and deduce the pile-top settlement (Bruce 1986, Mandolini *et al.* 2005, Semet 2016, Gullu *et al.* 2017). Accurate estimation of bearing capacity and settlement of pile foundation are the keys to ensure the safety of pile foundation. Many researchers illustrated that the post-grouting technique is a much validated method for eliminating the technological defects, improving the ground strength, and optimizing the parameters of bored piles (Fleming 1993, Mcvay *et al.* 2010). The study of the bearing capacity and settlement for the post-grouted pile have been investigated by several scholars in the previous work using different method: (a) analytical methods (e.g., Guo and Randolph 1999, Mullins *et al.* 2006, Zhang *et al.* 2012, Thiyyakkandi *et al.* 2012, Zhang *et al.* 2014, Wang *et al.* 2018, Li *et al.* 2019a, b), (b) numerical analysis (e.g., Danno 2009, Ni *et al.* 2010, Voottipruex 2011, Karimi *et al.* 2017, Castelli and Maugeri 2002, Zou *et al.* 2019) and (c) experimental investigations (Mullins 2006, Jardine 2009, Spagnoli *et al.* 2016, He *et al.* 2017). Analytical methods may be limited by some highly simplified assumptions that may cause the deviation of solutions from the true working state of piles. It also needs to be mentioned that the numerical simulation methods can be time-consuming and usually require a larger number of input variables, some of which should be estimated or assumed if not available at hand. A distinct advantage of the experimental methods lies in that the field data can provide meaningful physical insight into the governing parameters and also offer direct design data for pile engineers. Published literature has mainly investigated the settlement of the grouted pile by analytical methods (Guo and Randolph 1999, Danno 2009, Xia and Zou 2017) and numerical analysis (Feng and Lewis 1987, Maier and Gioda 1982, Hyodo *et al.* 2019). Only a few of literature have reported the long-term settlement of the cast-in-place bored pile by the field test method. For instance, Liu (2011) presented that the bearing capacity of the post-grouted pile is improved at least 70% than that of non-grouted piles. Thiyyakkandi *et al.* (2013) proposed a predict approach of the axial loading based on the performed experimental and FEM modeling. Thiyyakkandi *et al.* (2014) focused on the group-piles behavior of tip and side grouting. However, there are some differences in the calculation parameters between the laboratory test results and the field results. Chen *et al.* (2000) presented the direct back analysis method based on the displacement messages obtained from

*Corresponding author, Ph.D. Student
E-mail: yangtao@csu.edu.cn

ISSN: 2005-307X (Print), 2092-6219 (Online)

the constructing. Comodromos *et al.* (2009) obtained fitting values for soil shear strength, deformation modulus, and shear strength mobilization at the soil-pile interface.

Due to the fact that the experimental methods, compared with the numerical simulations and analytical methods, can provide meaningful physical insight into the governing parameters and also offer direct design data for pile grouting. Laboratory tests are carried out to measure the strength and deformation parameters of local soil sample. The six engineering bored piles (two non-grouted piles, two post-tip-grouted piles, a post-side-grouted pile, and a tip and side post-grouted pile) and three test bored piles (a tip post-grouted piles, a post-side-grouted pile, and a tip and side post-grouted pile) are installed to study the pile-top settlement, the axial force and side friction resistance under the axial loading. Finally, the settlement data obtained by field test are used for the back analysis and numerical calculation to predict the long-term settlement of the cast-in-place bored pile reinforced by post-grouting. In this paper, the results from a field test of the post grouted pile in the deep-thick soft soil are presented, and a novel prediction method for the long-term settlement of the post grouted piles is proposed. The test results and the proposed method can provide some direct design data and practical guidance for post grouting pile design.

2. Laboratory test

In order to predict the long-term settlement of the post-grouted piles, laboratory tests (i.e., liquid limit and plastic limit test, compression-deformation test, direct shear test and triaxial test of grouted soil) are carried out. The results of the laboratory test are expressed as follows.

2.1 Soil sampling and soil layer distribution

Four boreholes (i.e., 482 #, 489 #, 497 #, 503 # pile borehole) are set at the field. A set of soil samples are taken at 2.0 m between two adjacent boreholes, and one group of soil samples are obtained at the bottom of drilling hole, the undisturbed soil sample has a diameter of 80 mm and a height of 200 mm. The soil sample number is “ABC-XX”, where “ABC” means the pile number, “XX” means the depth of the soil sample. For example, “482” represents the number of piles, and “4” denotes the depth of soil layer in the number”482-4”. For the layout of piles, soil sample collection and static load test location are shown in Fig. 1, and the soil layer distribution and grouting range are shown in Fig. 2.

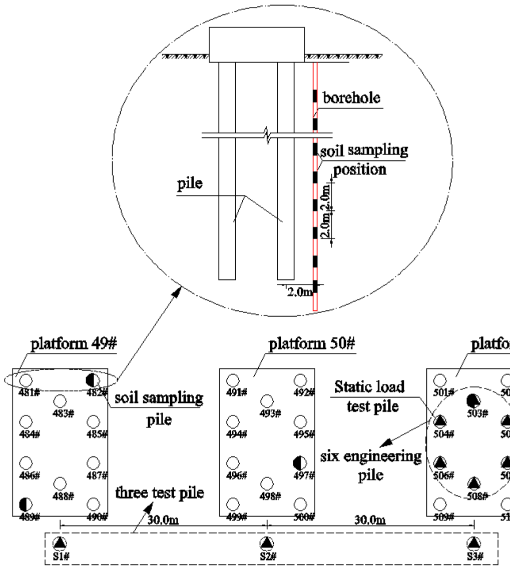

Fig. 1 Pile layout diagram containing sampling and static load test location information

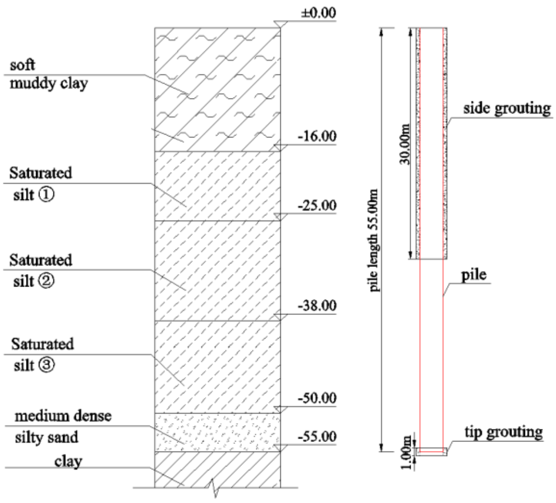

Fig. 2 The soil distribution and grouting range

2.2 Compression-deformation

Consolidometer is used for carrying out the compression-deformation test by step-wise loads. The vertical load imposed on the soil sample is 50 kPa, 100 kPa, and 200 kPa, respectively. The stability standard for each load is that the soil layer deformation ratio is less than 0.01 mm/h. Test results are shown in Fig. 3. The pressure in the legend of Fig. 3 is the confining pressure (σ_3).

It is known from the test results that the compression modulus of the in-site soil sample will increase with the ratio of cement increasing. Compression modulus is constrained modulus which represents the ratio of vertical stress to vertical strain under the lateral strain condition. When the cement content exceeds 40% (i.e., 40 percent of cement slurry by weight of soil in wet condition) the compression modulus approximately keeps stable. When the cement content is less than 20%, vertical stress has no significant effect on the compression modulus. The compression modulus of one soil layer will increase with the vertical stress increasing.

Direct shear test is carried out to measure the shear strength of soil sample and soil sample with cement. The soil-cement specimen is made of undisturbed soil sample 497# mixed with 2%, 5% and 10% of cement slurry by weight of soil, respectively. Results are shown in Fig. 4.

One can infer from Fig. 4 that the cohesion c generally decreases with the increase of the depth, but the shear strength of the soil sample with cement is obviously

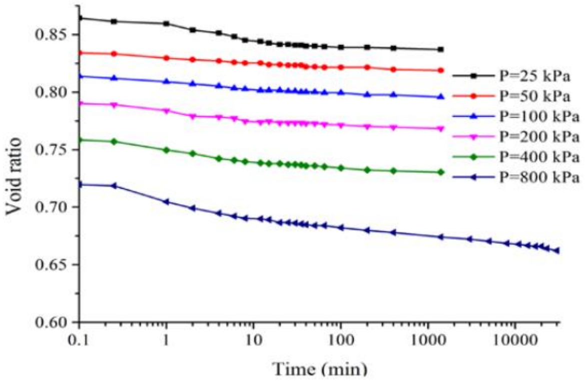

(a) Compression curves of 497-32

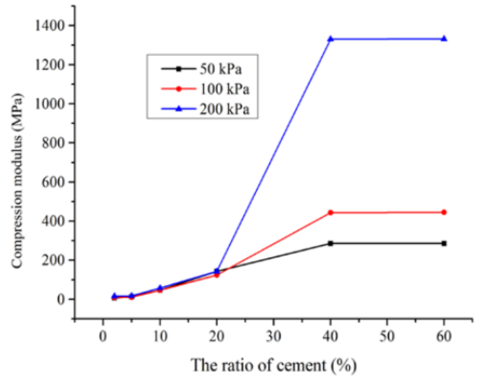

(b) Compression modulus under the different ratio of cement

Fig. 3 Compression curves and compression modulus under the different ratio of cement of 497-32

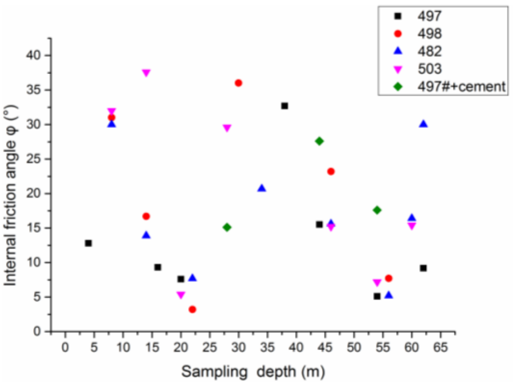

(a) Internal friction angle

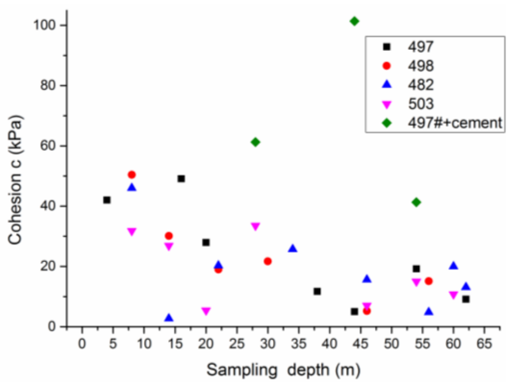

(b) Cohesion

Fig. 4 Shear strength of soil sample and soil sample with cement corresponding to sampling depth

improved. In addition, the increase of cohesion c is larger than that of internal friction angle.

2.4 Rheological test

Rheological test is conducted with a consolidometer. The volume of the soil sample is 30 ×2×2 cm. under each load reaches to a state of steady step-wise loading method is adopted and the load grades are 25 kPa, 50 kPa, 100 kPa, 200 kPa, 400 kPa, 800 kPa and 1600 kPa, respectively. Each load reaches a steady state and keeps 24 h. Results are shown in Fig. 5.

The results show that the secondary consolidation coefficient of grouting soil is less than natural soil. It indicates that grouting could improve the compression and rheological property of soil.

3. Filed test

By post-grouting, bearing capacity and lateral resistance of pile are improved. In this test, six engineering bored piles and three test bored piles are selected to obtain the engineering properties and long-term settlement of the post-grouting pile.

3.1 Grouting mode

In order to obtain the long-term settlement and engineering characteristics of the post-grouting pile under the different post-grouting methods, three post-grouting methods (i.e., post-tip-grouting, post-side-grouting, and tip and side post-grouting) are designed and carried out by field tests. Post-tip-grouting is only grouting at the tip of the cast-in-place pile, and the grouting length is 1.0m. Post-side-grouting is only grouting at the side of the cast-in-place pile, and the grouting length is 30.0m. Tip and side post-grouting is grout at the tip and side of the cast-in-place pile. The grouting range and soil layer distribution are shown in Fig. 2. The grouting material is cement slurry with a water cement ratio of 0.6:1. Grouting pressure varies from 0.5 to 2.5 MPa. The volume of grouting is measured by the flowmeter, and then the grouting weight is converted by grouting density. The grouting pressure and grouting volume of each pile are shown in Table 2. In Table 2, tip and side 1.5 t means that 1.5 t of grouting material is injected at pile tip and another 1.5 t is injected along the pile shaft.

3.2 Field test project

The static load test was performed under a slow procedure which can be found in Technical Code for Testing of Building Foundation Piles. The maximum load of the jack is 1.3 times the design load of the pile. Settlement and stresses at tip or side of piles are measured by the displacement sensor and the vibrating wire rebar stress meter, and the corresponding technical parameters can be

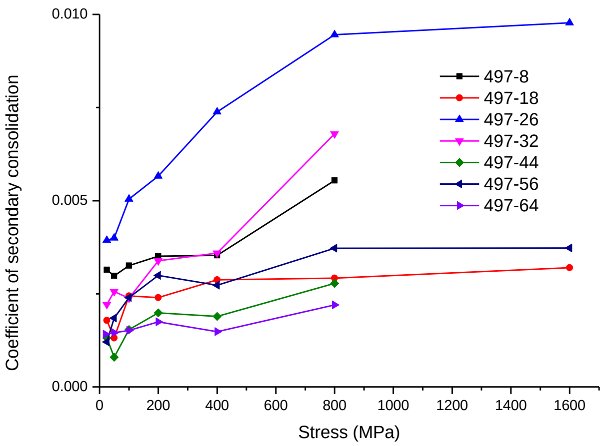

(a) Pile 497

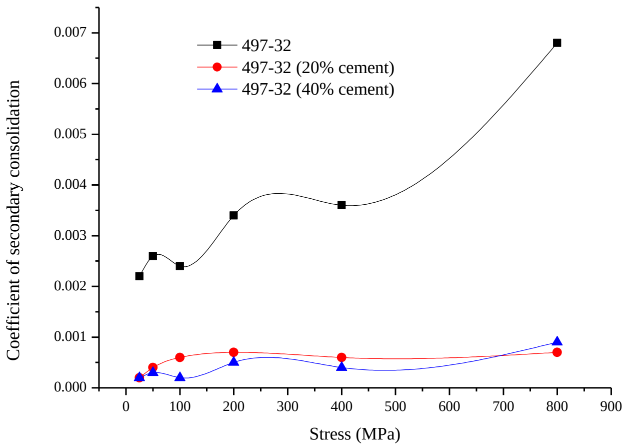

(b) Pile 497 with different cement

Fig. 5 Relationships between the secondary consolidation coefficient and the stress of the pile 497

Table 1 Technical parameters of the steel stress meter

Model	JTM-V1000D-100	
Measurement range	Maximum pull stress, 100MPa	Maximum pressure stress, (200MPa)
Resolution ratio %/F•S	≤0.14	≤0.07

(a) Reserved grouting pipe

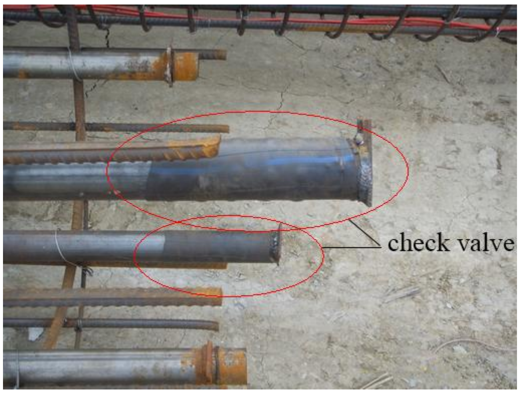

(b) Check valve

(c) Side grouted pipe

(d) Stress meter

Fig. 6 Grouting pipe and steel stress meters

noticed in Table 1. The vibrating wire rebar stress meter is welded on the rebar to measure the strain of the rebar, and then the strain can be converted into stress using the elastic modulus (i.e., E=2.0GPa) of the rebar, as is shown in Fig. 7.

For each pile, 48 vibrating wire rebar stress meters are embedded at tip and side of the piles. There are 12 cross-sections along the depth of pile and the spacing is 4 meters and 6 meters respectively. Four steel stress meters are installed in every cross-section along the diameter of the pile. The grouting pipe and vibrating wire rebar stress

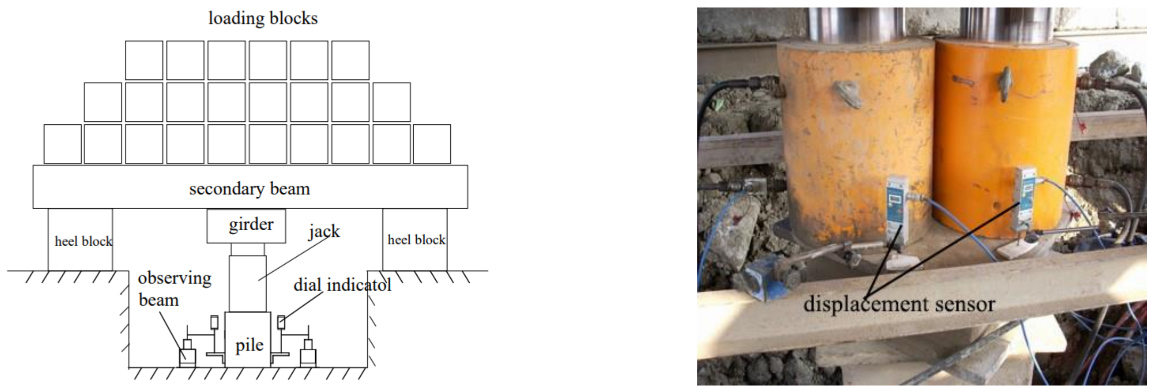

(a) Schematic diagram of the static loading test (b) Jack and sensor

Fig. 7 Field static loading test

Table 2 Grouting parameters

Number	503#	504#	505#	506#	507#	508#	S1	S2	S3
Length (m)	55								
Diameter (m)	1								
Grouting method	Tip and side	Tip	No	No	Tip	Side	Tip	Side	Tip and side
Grouting quantity (t)	1.5	3	-	-	3	3	3	3	1.5
Grouting Pressure(MPa)	1~1.5	0.5~1	-	-	1.5	1~2.5	1.5	1~5.5	1~1.5

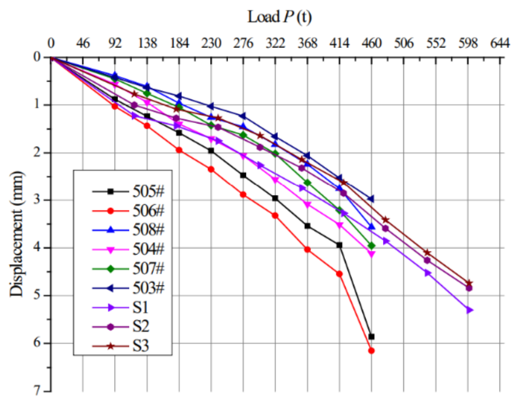

Fig.8 Loading-displacement curves

Table 3 Settlement decrement because of the post-grouting

Settlement decrement (%)	508#	504#	507#	503#	S1	S2	S3
	Side grouting	Tip grouting	Tip grouting	Tip + side grouting	Tip grouting	Side grouting	Tip + side grouting
Compared with 505#	22.20%	30.10%	32.90%	32.40%	9.56%	17.43%	19.12%
Compared with 506#	25.80%	33.20%	35.98%	35.50%	13.92%	21.37%	22.98%

meters are shown in Fig. 6.

3.3 Post-grouting test

Post-grouting parameters for six engineering cast-in-place bored piles and three test cast-in-place bored piles are shown in Table 2. The test pile is set only for static load test with large loads, and its maximum test load is 600t. The engineering pile will be used as the foundation of the bridge after the static load test, and the test can only be carried out with 1.3 times larger than the design load, and the maximum test load is 460t. Besides the maximum test load, there are no differences between these two groups.

As shown in Fig. 7 (a), the mass load of the loading blocks is transmitted to the girder through the secondary beam, and the step by step load is applied to the top of the pile by a jack. The displacement meter is fixed on the observing beam to measure the displacement of the pile. The static load test was performed under a slow procedure which can be found in Technical Code for Testing of

Building Foundation Piles (English Version). For engineering cast-in-place bored piles, the maximum loading is 460 t and the load grade is 92 t, 138 t, 184 t, 230 t, 276 t, 322 t, 368 t, 414 t and 460 t, respectively. For test cast-in-place bored piles, the maximum loading is 600 t. The load grade is 120 t, 180 t, 240 t, 300 t, 360 t, 420 t, 480 t, 540 t and 600 t, respectively. The waiting times between each step of the load shall not be less than 2h. The test apparatus is shown in Fig. 7.

3.4 Field test project

Four displacement sensors are installed symmetrically on the top of piles to obtain the pile-top settlement. Loading-displacement curves are shown in Fig. 8.

It is known from Fig. 8 that the settlement of 505# and 506# are, respectively, 5.89 mm and 6.17 mm when the load is 460 t. The settlement comparisons between 505# and 506# with other piles are shown in Table 3. When the loading is less than 414 t, the loading-settlement curves of all piles are nearly linear. When the loading is more than 414 t, the settlement-loading curves of 505# and 506# have a grammatically dropping, whereas the curves of other piles still keep linear. The reason why settlement-loading curves of 505# and 506# have a grammatically dropping is that the 414 t load exceeds the ultimate bearing capacity of the un-grouting pile foundation. While the ultimate bearing capacity of grouting piles was improved by the post-grouting technique, and exceeds 414 t. So the curves of grouting piles still keep linear. It can be inferred that the post-grouting technique is able to improve the engineering characteristic and decrease settlement of the pile.

When the loadings of six engineering bored piles and three test bored piles are 460 t and 600 t, respectively the axial force-depth curves and the friction resistance-depth curves are obtained by the vibrating wire rebar stress meters. Test curves are shown in Fig. 9 and Fig.10.

It can be seen from Fig. 9 that the axial force of the pile decreases as the depth increases, and its value is close to zero at the bottom of the pile. It indicates that the friction resistance of the soil on the bottom pile is not fully mobilized, and the pile has not reached its ultimate bearing capacity. Further analysis of the descending trend of axial force in six engineering piles shows that the rate of descent of all piles at 0-15 m (i.e., clay) is basically the same, but the rate of decrease of side grouting pile (i.e., 503, 508) is faster than that of un-grouting pile under 15 m (i.e., silt). The main reason may be that the grouting effect is better in silt than in clay, and the lateral friction resistance of the silt after grouting is easier to be mobilized.

In Fig. 10, the distribution and value of the resistance of the un-grouted piles (505#, 506#) and the side grouting piles (503#, 508#) in different layers are compared. It can be inferred that the resistance has little change at the range of 0.0-15.0 m (i.e., clay), but rises sharply at 15.0-30.0 m (i.e., silt). It is concluded that the grouting effect in the silt is much better than that in the clay.

When the loading P=460 t, the side friction resistance of 505# and 506# accounts for 91.304% and 89.565% of the total loading and the max friction resistance is 42.2 kPa and 41.4 kPa, respectively. The max friction resistance of 508# is 55.7 kPa, which improves about 33% compared with the max friction resistance of 505# and 506#. The side friction resistance of 508# accounts for 94.565% of the loading. The tip resistance of 504# and 507# accounts for 6.957% and 7.609% of the loading, while the tip resistance of 505# and 506# accounts for 8.696% and 10.435% of the loading. The tip resistance of 503# accounts for 4.348% of the loading. The friction resistance improves with the increment of grouting which could be known as the increment of pile base, the results show in agreement with the discussion in Zhang, *et al.* (2013) (i.e., an increase in the material strength at the pile base puts significant and positive impact on mobilizing the shaft resistance).

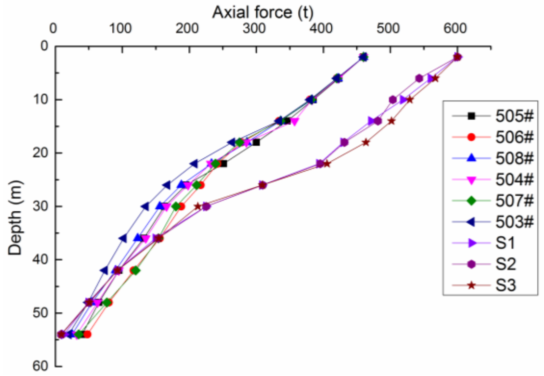

Fig. 9 Axial force-depth curves

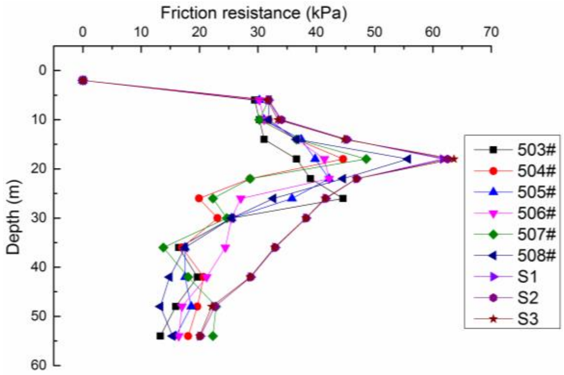

Fig. 10 Unit skin friction resistance-depth curves

When the loading P=600 t, the max resistance of S1, S2 and S3 appears at 18 m below pile-top, which accounts for 61.70 kPa, 62.50 kPa and 63.60 kPa. The tip resistance of S1, S2 and S3 is 61.7 kPa, 62.5 kPa and 63.60kPa, which just accounts for respectively 10.283%, 10.417% and 10.6% of the loading.

4. Parameters back analysis and prediction of long-term settlement

Non-grouted piles 505# and 506#, side-grouted piles 508#, tip-grouted pile 504# and 507#, and the tip and side grouted pile 503#, three cast-in-place bored test piles (i.e., S1, S2 and S3) are selected as the back analysis objects.

4.1 Field settlement data

The collection of the field settlement data is conducted

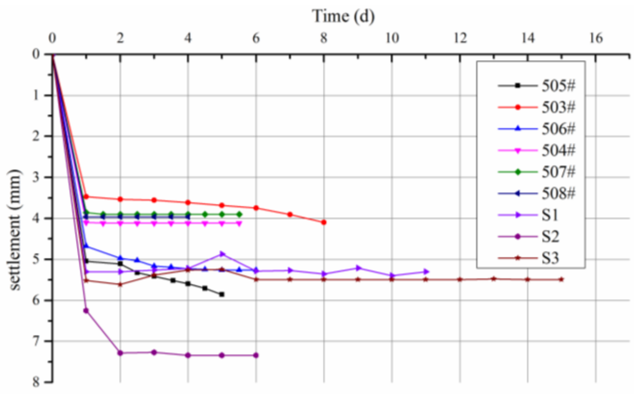

Fig. 11 Settlement-time curves

Table 4 Parameters of the different soil layers

Soil layer	Thickness *h* (*m*)	Bulk density *γ* (*kN/m³*)	Cohesion *c* (*kP*)	Internal friction angle *φ*	Compression modulus *Es* (*MPa*)	Poisson's ratio *ν*
Muddy clay	0-16	18.3	8	19.5	22.7	0.38
silt ①	16-25	17.7	10	9	24.8	0.33
silt ②	25-38	18.4	11	15	41.5	0.33
silt ③	38-50	20	33	15	91.5	0.35
sand	50-55	19.5	3	27.5	271.8	0.28

in the process of the pile static load test. In order to study the long-term settlement of the pile foundation under creep conditions, the static load test was performed under the slow procedure to reach the maximum load and then maintain the maximum load for 5-15 days. The displacement of the pile was measured by sensor every day. By field tests, the settlement-time curves of six engineering cast-in-place bored piles under the maximum loading P=460 t and three cast-in-place bored test piles under the maximum loading P=490 t are shown in Fig. 11.

4.2 Selection of the back analysis parameters

The parameters of the cast-in-place bored piles are obtained by laboratory test (i.e., liquid limit and plastic limit test, compression-deformation test, direct shear test and triaxial test of grouted soil). The pile length L is 55.0 m, diameter d is 1.0 m. The Poisson's ratio ν is 0.2, Elastic Modulus E is 31.5 GPa. As shown in Table 4, the pile goes through five different soil layers which are clay, silt soil ①, silt ②, silt ③ and sand, the bottom of piles is clay. Parameters of the different soil layers are shown in Table 4.

In order to simplify the calculation, cast-in-place bored pile and soil are considered as a homogeneous material. The parameters in the FLAC3D are selected as that bulk density γ=19.0 kN/m3, cohesion c=20 kPa, internal friction angle φ=15°. Shear modulus and bulk modulus are calculated by the Eq. (1) and Eq. (2).

$$G = E / 2(1+\nu) \tag{1}$$

$$K = E / 3(1-2\nu) \tag{2}$$

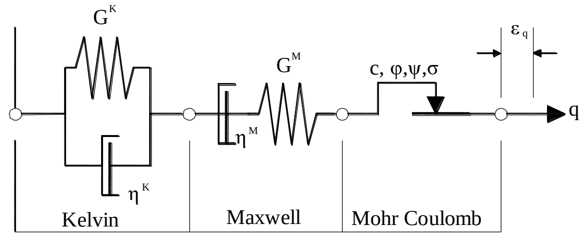

Fig. 12 Schematic representation of CVISC model

where, *ν* is Poisson's ratio, E is elasticity modulus and can be expressed by

$$E = E_s / \left[1 - 2\nu^2 / (1-\nu)\right] \tag{3}$$

According to Eqs. (1)-(3), the shear modulus G=10 MPa, and bulk modulus K=30 MPa are selected as the one back analysis parameter.

The CVISC creep model is taken into account based on the Mohr-Coulomb failure criterion, which has three control parameters (Maxwell dynamic viscosity m_s, Kelvin shear modulus k_s, Kelvin viscosity k_v). k_s is selected as a back analysis parameter, and let m_s = k_v, the value of k_s is selected based on the settlement of the grouted piles and non-grouted piles. In this paper, two back parameters are selected, one is the bulk modulus K, the other is the creep parameter k_s.

4.3 Prediction model

The CVISC creep model is a Viscous-elastic-plastic Model of FLAC3D, and the model has been proven to be effective in predicting long-term settlement of foundations under creep conditions. Jiang *et al.* (2013) adopt the CVISC creep model to simulate subgrade settlement after construction. The CVISC model also (Pellet 2009, Bonini *et al.* 2009, Sharifzadeh *et al.* 2013) adopted for modeling time-dependent behavior of the weak hosting rock mass. The CVISC model in FLAC is characterized by a visco-elasto-plastic deviatoric behavior, as shown in Fig. 12. The visco-elastic constitutive law corresponds to a Burger model (Kelvin cell in series with a Maxwell component), and the plastic constitutive law corresponds to a Mohr-Coulomb model. In this model, the visco-elastic strains are deviatoric and depend only on the deviatoric stress $D_{i,j}$, instead the plastic strains are both deviatoric and volumetric and depend on σ_{ij} in accordance with the chosen flow rule (Bonini *et al.* 2009).

For the CVISC model, the deviatoric strain rate partitioning is expressed as

$$\dot{\varepsilon}_{ij} = \dot{\varepsilon}_{ij}^{K} + \dot{\varepsilon}_{ij}^{M} + \dot{\varepsilon}_{ij}^{P} \tag{4}$$

Constitutive laws of the deviatoric behavior for Kelvin unit are expressed as follows

$$D_{ij} = 2\eta^{K}\dot{\varepsilon}_{ij}^{K} + 2G^{K}\dot{\varepsilon}_{ij}^{K} \tag{5}$$

For Maxwell unit,

$$\dot{\varepsilon}_{ij}^{M} = \frac{\dot{D}_{ij}}{2G^{M}} + \frac{D_{ij}}{2\eta^{M}} \tag{6}$$

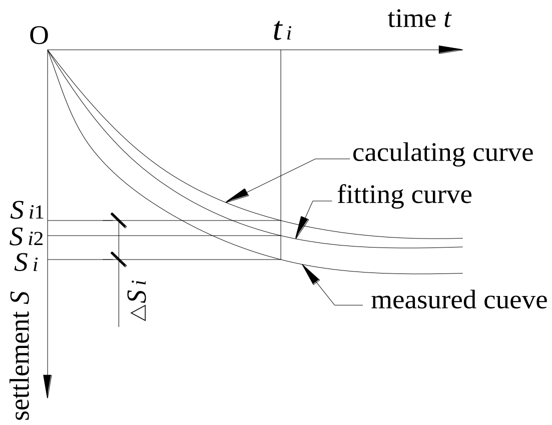

Fig. 13 Settlement- time curves under loading

For Mohr-Coulomb Plastic unit,

$$\dot{\varepsilon}_{ij}^{\mathrm{P}} = \lambda * \frac{\partial g}{\partial \sigma_{ij}} - \frac{1}{3}\dot{\varepsilon}_{\mathrm{vol}}^{P}\delta_{ij} \tag{7}$$

where,

$$\dot{\varepsilon}_{\mathrm{vol}}^{P} = \lambda * \left[\frac{\partial g}{\partial \sigma_{11}} + \frac{\partial g}{\partial \sigma_{22}} + \frac{\partial g}{\partial \sigma_{33}} \right] \tag{8}$$

The constitutive laws of the volumetric behavior are formulated as follows

$$\dot{\sigma}_0 = K(\dot{\varepsilon}_{vol} - \dot{\varepsilon}_{\mathrm{vol}}^{P}) \tag{9}$$

In the above Eqs. (4)-(9), the superscripts M, K and P represent the Kelvin unit, Maxwell unit and Mohr-Coulomb plastic unit of the corresponding parameters; the parameters with superscripts dot donate their first differential corresponding to rheological time. The K is bulk modulus, G is shear modulus and η are the dynamic viscosity. The D_{ij} and σ_{ij} are the deviatoric components derived from the strain and stress tensors, respectively; ε_{vol} and σ_0 are the volumetric components of the strain and stress tensors. $\lambda^*$is a multiplier that can be eliminated in the calculation afterwards.

In the Mohr-Coulomb plastic model, the failure criterion f is expressed as follows

$$f = \sigma_1 - \sigma_3 N_\phi + 2C\sqrt{N_\phi} \tag{10}$$

where, c is the cohesion, ϕ is the friction angle and parameter N_ϕ=(1+sinϕ)/(1-sinϕ).

The plastic potential function g as shown by

$$g = \sigma_1 - \sigma_3 N_\varphi \tag{11}$$

where, σ_1 and σ_3 are the major and the minor principal stresses; φ is the dilation angle and parameter N_φ=(1+sinφ)/(1-sinφ).

4.4 Parameters back analysis

The analysis method of the nonlinear settlement-time curve is selected, which takes the pile-soil surface and the soil under the pile bottom into consideration. Procedures of the method are shown as follows.

(1) In Fig. 11, when loading P=460t, non-grouted pile 505# is selected as an example to illustrate the parameters back analysis and the static creep test. Firstly, select the settlement of the first day and the last day as the fitting magnitude of back analysis. Then, select a group values of bulk modulus K and creep parameter ks: $\{x_j\} = \{x_1, x_2\} = \{K, k_s\}$.

(2) Choose n points from the settlement-time curve, therefore, time of the n points and corresponding n settlement values are obtained.

On settlement-time curves, when loading P at time ti, the corresponding settlement Si1 is obtained by numerical simulation, where, Si1 is the settlement value of numerical calculation corresponding to time ti, Si2 is the fitting settlement results corresponding to time ti, as shown in Fig. 13. Define

$$f(P, K, k_s, t_i) = S_{i1} \tag{12}$$

where, $f(P, K, k_s, t_i)$ is a function of settlement, varies with soil mechanical parameters, loading P and time t_i are constant values.

$$\frac{\partial f}{\partial P}\cdot dP + \frac{\partial f}{\partial \mathrm{K}}\cdot dK + \frac{\partial f}{\partial k_s}\cdot dk_s + \frac{\partial f}{\partial t_i}\cdot dt_i = dS_i \tag{13}$$

As for constant loading P and time t_i, there are dP=0 and dt_i=0. Fig. 9 shows that the difference between measured settlement and the calculating result is ΔS_i under loading P. There is

$$\begin{cases} \left[\frac{\partial f}{\partial K}\right]_{(P,\ t_1)} \cdot dK + \left[\frac{\partial f}{\partial k_s}\right]_{(P,\ t_1)} \cdot dk_s = \Delta S_1 \\ \left[\frac{\partial f}{\partial K}\right]_{(P,\ t_2)} \cdot dK + \left[\frac{\partial f}{\partial k_s}\right]_{(P,\ t_2)} \cdot dk_s = \Delta S_2 \\ \mathrm{M} \qquad\qquad \mathrm{M} \qquad\qquad \mathrm{M} \\ \left[\frac{\partial f}{\partial K}\right]_{(P,\ t_n)} \cdot dK + \left[\frac{\partial f}{\partial k_s}\right]_{(P,\ t_n)} \cdot dk_s = \Delta S_n \end{cases} \tag{14}$$

Eq (3) is rewritten as a matrix and is shown in Eq. (4).

$$[A]\cdot\{dx_j\} = [dS_i] \tag{15}$$

where,

$[A] = \begin{bmatrix} A_{11} & A_{12} \\ A_{21} & A_{22} \\ \vdots & \vdots \\ A_{n1} & A_{n2} \end{bmatrix}$ and $A_{11} = \left[\frac{\partial f}{\partial K}\right]_{(P,\ t_i)}$, $A_{12} = \left[\frac{\partial f}{\partial K}\right]_{(P,\ t_i)}$. $A_{ij} = \left[\frac{\partial f}{\partial x_j}\right]_{xi}$,

The element A_{ij} donate the sensitivity of settlement to

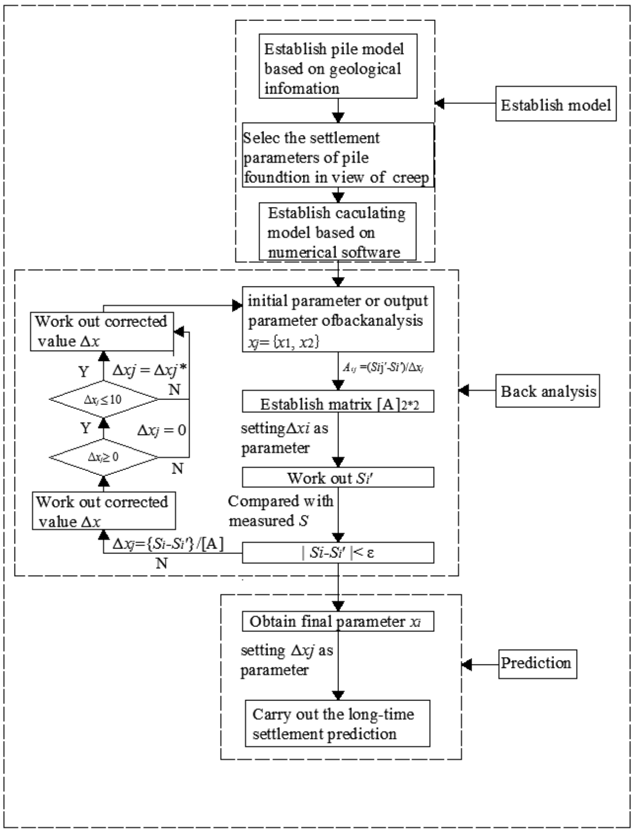

Fig.14 Calculation process of numerical simulation

Table 5 Results of the back analysis

Number	Assumed creep parameters		The initial back analysis parameters		The final back analysis parameters		Back analysis times	Difference between back analysis and measurement
	m_s ($Pa{\cdot}s$)	k_v ($Pa{\cdot}s$)	k_s ($Pa{\cdot}s$)	K (Pa)	k_s ($Pa{\cdot}s$)	K (Pa)		
503#	1.5×10⁹ → 1.5×10^9	1.5×10^9	1.15×10^9	3.31×10^7	1.15×10^9	3.313×10^7	1	
504#	1.5×10^9	1.5×10^9	1.1×10^9	3.3×10^7	1.145×10^9	3.3×10^7	2	
505#	5.0×10^8	5.0×10^8	6.8×10^8	3.0×10^7	6.8×10^8	3.0×10^7	1	
506#	5.0×10^8	5.0×10^8	6.8×10^8	3.0×10^7	8.208×10^8	3.0×10^7	4	
507#	1.5×10^9	1.5×10^9	1.1×10^9	3.3×10^7	1.224×10^9	3.3×10^7	4	< 10%
508#	6.0×10^8	6.0×10^8	7.256×10^8	3.04×10^7	8.024×10^8	3.132×10^7	5	
S1	1.5×10^9	1.5×10^9	1.0×10^9	3.1×10^7	1.07×10^9	3.399×10^7	4	
S2	5.0×10^8	5.0×10^8	6.09×10^8	3.0×10^7	6.09×10^8	3.0×10^7	1	
S3	1.5×10^9	1.5×10^9	1.0×10^9	2.9×10^7	1.030×10^9	2.9×10^7	2	

the parameter x_j at a specified time point t_i under a certain load P. For $\{dx_j\}=\{dx_1, dx_2\}^T=\{dK, dk_s\}^T$, dx_j represents the adjusted value of the parameter x_j. For $\{\Delta S\}=\{\Delta S_1, \Delta S_2,\cdots, \Delta S_n\}^T$, ΔS_i is the difference between measured settlement and calculating settlement.

The calculating method of the matrix [A] is described as follows:

(1) Work out the S_{i1} at time t_i when loading is P under the condition of given parameters, where S_{i1} is the settlement calculation value corresponding to time t_i, as shown in Fig. 13.

(2) Make $x_j'=x_j+\Delta x_j$, work out the corresponding settlements S_{ij}, where S_{ij} is the settlement calculation value corresponding to the new parameter $x_j'=x_j+\Delta x_j$ and time t_i.

(3) According to the definition of A_{ij}, there is

$$A_{ij}=\frac{S_{ij}'-S_i'}{\Delta x_j}, \tag{16}$$

(4) Work out the corresponding A_{ij} when j= 1, 2 based on the mentioned method.

(5) In Fig. 8, when loading P=460t, non-grouted pile 505# is selected as an example to illustrate the parameters back analysis and the static creep test. Then select the

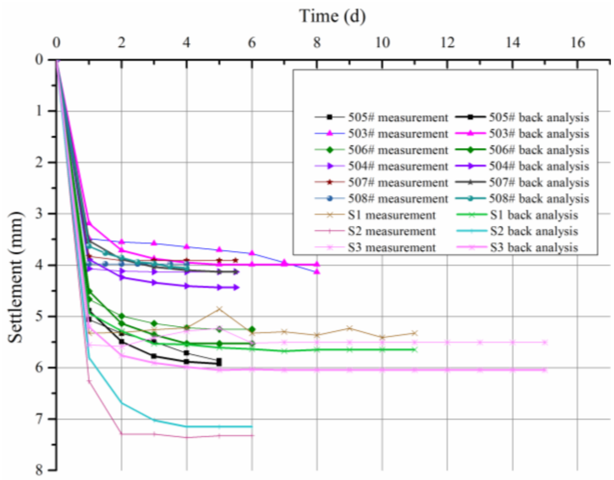

Fig. 15 Comparisons between the back-analysis curves with the measured curves

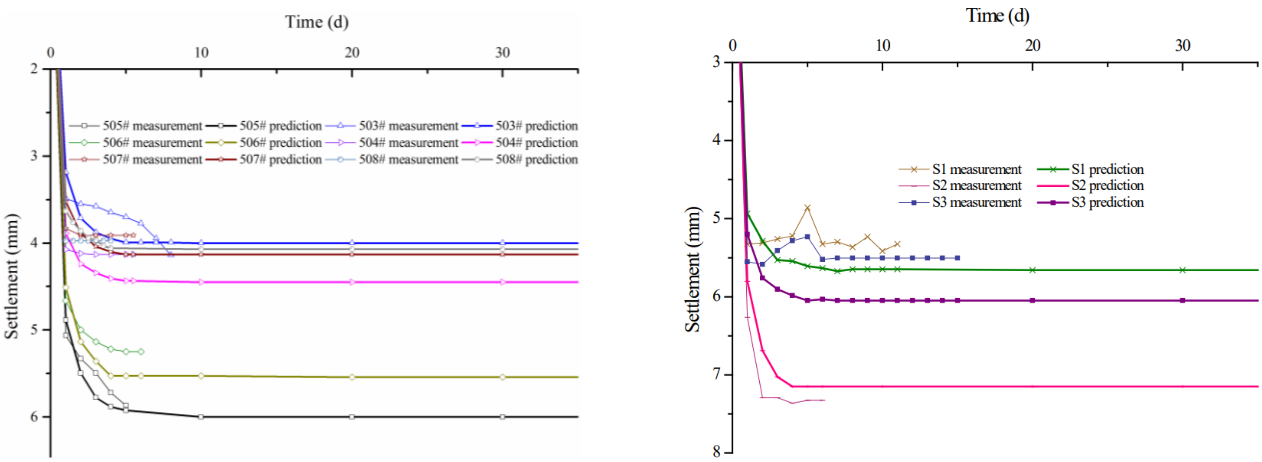

(a) For six engineering cast-in-place bored piles

(b) For three test cast-in-place bored piles

Fig.16 Comparison between the long-term settlement prediction curves with the measured curves

settlement of the first day and the last day as the fitting magnitude of back analysis. All the elements in the matrix [A] can be worked out let i=1, 2. In that case, one can obtain a 2×2 matrix A.

It should be noted that Δx_j=10% x_j when working out A_{ij}. By solving the equation $[A]\cdot\{dx_j\}=[dS_i]$, $\{dx_j\}$ could be obtained. Let $\{x_j\}'=\{x_j\}+\{dx_j\}$, then use $\{x_j\}'$ to calculate a new settlement-time curve. The new settlement-time curve will be closer to the measured curve compared with the curve obtained by previous parameters. This method is used to fit the settlement data until the required precision is achieved. The calculation processes are shown in Fig. 14.

4.5 Numerical calculation process

FLAC^{3D} is used to predict the long-term settlement of the pile. A pile-soil model considering creep is proposed to carry out back analysis and the process is shown in Fig. 14.

$\triangle x_j$* is the corrected value needed in back analysis when fitting the measured settlement curves and the settlement curves obtained by the back analysis parameters x_j and $x_j+\triangle x_j(\triangle x_j=10\%x_i)$. When $\triangle x_j>0$, if the corrected value of x_j is not tended to the measured value, do not need to correct x_j. If both x_j and $x_j+\Delta x_j$ (Δx_j=10%x_j) are not tend to the measured value, x_j should be appropriately adjusted.

4.6 Prediction results

The results of the back analysis are shown in Table 5.

The final back analysis parameters are applied into the numerical calculation to get the back-analysis curves. The comparison between the back-analysis curves and the measured curves are shown in Fig. 15.

By studying the settlement-time curves, the back analysis data of the bulk density K and creep parameter k_s, are obtained, the final settlement difference between back analysis and measurement is presented to be between 1.11% and 7.41%. The settlement trend obtained by back analysis technique is in accord with the measured settlement trend. Consequently, the prediction model could carry out the long-term settlement prediction under the static loading.

The long-term settlement prediction curves are shown in Fig. 16. By comparing the results of the back analysis and measurement in Fig. 15 and Fig. 16, the prediction is available under the condition of long-term creep of piles in this paper. The settlement caused by the creep of the un-grouted piles 505# and 506# accounted for 1.2% and 0.9% of the total settlement, respectively. In addition, the average settlement caused by the creep of the grouted piles (i.e., 503#, 504#, 507#, 508#, S1#, S2#, S3#) accounted for 0.4% of the total settlement. The settlement of the pile reaches a maximum at 20-30 days, and the settlement prediction curve approach a constant value when the number of days exceeds 30 days. In engineering practical applications, for 460 t load, the number of days required to eliminate long-term settlement of the cast-in-place bored pile which reinforced by post-grouting technique is 30 days.

5. Conclusions

This paper presents a series of laboratory test and field test to investigate the long-term settlement and stress behavior of six engineering cast-in-place bored piles and three cast-in-place tests bored piles reinforced by post-grouted technique. The following conclusions could be deduced from the results.

(1) For six engineering piles, when loading is 460 t, post-side-grouted will decrease the settlement by 22.2%-25.8%, the tip and side post-grouting will decrease the settlement by 32.4%-35.5%, and post-tip-grouting will decreasing the settlement by 30.1%-35.98%.

(2) When loading is 460 t, the side friction resistance of non-grouted piles 505# and 506# respectively accounts for 91.3% and 91.74% of the total loading. The proportions of the side friction resistance for post-side-grouted pile 508#, post-tip-grouted piles 504# and 507#, and the tip and side post-grouted pile 503# are 95.7%, 93.91%, 93.04%, and 93.04%, respectively.

(3) The back analysis approach for the long-term settlement is presented with the control parameters of the bulk modulus K and the creep parameter k_s. The final settlement difference between back analysis and measurement is 1.11%-7.41%.

Acknowledgments

This work was supported by the Guizhou Provincial Science and Technology Major Project, No. Qian-ke-he-zhong-da-zhuan-xiang-zi [2018]3010.

References

Bonini, M., Debernardi, D., Barla, M. and Barla, G. (2009), "The mechanical behaviour of clay shales and implications on the design of tunnels", *Rock Mech. Rock Eng.*, **42**(2), 361-388. https://doi.org/10.1007/s00603-007-0147-6.

Bruce, D.A. (1986), "Enhancing the performance of large diameter piles by grouting", *Ground Eng.*, **19**(4), 9-15. https://doi.org/10.1016/0148-9062(87)91441-0.

Castelli, F. and Maugeri, M. (2002), "Simplified nonlinear analysis for settlement prediction of pile groups", *J. Geotech. Geoenviron. Eng.*, **128**(1), 76-84. https://doi.org/10.1061/(ASCE)1090-0241(2002)128:1(76).

Çelik, S. (2016), "An experimental investigation of utilizing waste red mud in soil grouting", *KSCE J. Civ. Eng.*, **21**(4), 1-10. https://doi.org/10.1007/s12205-016-0774-0.

Chen, S.H., Chen, S.F., Shahrour, I. and Egger, P. (2000), "The feedback analysis of excavated rock slope", *Rock Mech. Rock Eng.*, **34**(1), 39-56. https://doi.org/10.1007/s006030170025.

Comodromos, E.M., Papadopoulou, M.C. and Rentzeperis, I.K. (2009), "Pile foundation analysis and design using experimental data and 3-D numerical analysis", *Comput. Geotech.*, **36**(5), 819-836. https://doi.org/10.1016/j.compgeo.2009.01.011.

Dai, G., Gong, W., Zhao, X. and Zhou, X. (2010), "Static testing of pile-base post-grouting piles of the Suramadu bridge", *Geotech. Test. J.*, **34**(1), 34-49. https://doi.org/10.1520/GTJ102926.

Danno, K. and Kimura, M. (2009), "Evaluation of long-term displacements of pile foundation using coupled FEM and centrifuge model test", *Soils Found.*, **49**(6), 941-958. https://doi.org/10.3208/sandf.49.941.

Fattah, M.Y., Al-Saidi, A.A. and Jaber, M.M. (2015), "Improvement of bearing capacity of footing on soft clay grouted with lime-silica fume mix", *Geomech. Eng.*, **8**(1), 113-132. https://doi.org/10.12989/gae.2015.8.1.113.

Fellenius, B.H., Harris, D.E. and Anderson, D.G. (2004), "Static loading test on a 45 m long pipe pile in Sandpoint, Idaho", *Can. Geotech. J.*, **41**(4), 613-628. https://doi.org/ 10.1139/t04-012.

Feng, Z.L. and Lewis, R.W. (1987), "Optimal estimation of in-situ ground stresses from displacement measurements", *Int. J. Numer. Anal. Meth. Geomech.*, **11**(4), 391-408. https://doi.org/10.1016/0148-9062(88)92931-2.

Field, I.S.O. and Testing, L. (1985), "Axial pile loading test-Part 1: Static loading", *Geotech. Test. J.*, **8**(2), 12. https://doi.org/10.1016/0148-9062(86)91847-4.

Fleming, W.G.K. (1993), "The improvement of pile performance by base grouting", *Civ. Eng.*, **97**(2), 88-93. https://doi.org/10.1680/icien.1993.23262.

Gullu, H. (2017), "A new prediction method for the rheological behavior of grout with bottom ash for jet grouting columns", *Soils Found.*, **57**(3), 384-396. https://doi.org/ 10.1016/j.sandf.2017.05.006.

Guo, W.D. and Randolph, M.F. (1999), "An efficient approach for settlement prediction of pile groups", *Géotechnique*, **49**(2), 161-179. https://doi.org/ 10.1680/geot.1999.49.2.161.

He, B., Wang, L. and Hong, Y. (2017), "Field testing of one-way and two-way cyclic lateral responses of single and jet-grouting reinforced piles in soft clay", *Acta Geotechnica*, **12**(5), 1021-1034. https://doi.org/10.1007/s11440-016-0515-z.

Hyodo, J., Shiozaki, Y., Tamari, Y., Ozutsumi, O. and Ichii, K. (2019), "Modeling of pile end resistance considering the area of influence around the pile tip", *Geomech. Eng.*, **17**(3), 289-296. https://doi.org/10.12989/gae.2019.17.3.289.

Jardine, R.J., Zhu, B., Foray, P. and Dalton, C.P. (2009), "Experimental arrangements for investigation of soil stresses developed around a displacement pile", *Soils Found.*, **49**(5), 661-67.

Jiang, Z.B., Jiang, A.N. and Shi, J. (2013), "Subgrade settlement using CFG piles based on cvisc creep model", *Chin. J. Geotech. Eng.*, **35**(zk2), 346-351.

Karimi, A. H., Eslami, A., Zarrabi, M. and Khazaei, J. (2017), "Study of pile behavior by improvement of confining soils using frustum confining vessel", *Scientia Iranica*, **24**(4), 1874-1882. https://doi.org/10.24200/sci.2017.4278.

Kitiyodom, P., Matsumoto, T. and Kanefusa, N. (2004), "Influence of reaction piles on the behaviour of a test pile in static load testing", *Can. Geotech. J.*, **41**(3), 408-420. https://doi.org/10.1139/t03-098.

Li, C. and Zou, J.F. (2019a), "Closed-form solution for undrained cavity expansion in anisotropic soil mass based on the spatially mobilized plane failure criterion", *Int. J. Geomech.*, **19**(7), https://doi.org/10.1061/(ASCE)GM.1943-5622.0001458.

Li, C., Zou, J.F. and Zhou, H. (2019b), "Cavity expansions in k0 consolidated clay", *Eur. J. Environ. Civ. Eng.*, https://doi.org/10.1080/19648189.2019.1605937.

Liu, J.F. and Cui, X.Q. (2011), "Pile bearing capacity improvement by post-grouting on tip and side", *Adv. Mater. Res.*, **261-263**, 1313-1318. https://doi.org/10.4028/www.scientific.net/amr.261-263.1313.

Maier, G. and Gioda, G. (1982), *Optimization Methods for Parametric Identification of Geotechnical Systems*, in *Numerical Methods in Geomechanics*, Springer, The Netherlands, 273-304.

Mandolini, A., Russo, G. and Viggiani, C. (2005), "Pile foundations: Experimental investigations, analysis and design", *Proceedings of the 16th International Conference on Soil Mechanics and Geotechnical Engineering*, Osaka, Japan, September.

Mcvay, M., Thiyyakkandi, S., Joiner, J. and Adams, V. (2010), "Group efficiencies of grout-tipped drilled shafts and jet-grouted piles", No. UF Project 73980/74027.

Mullins, G., Winters, D. and Dapp, S. (2006), "Predicting end bearing capacity of post-grouted drilled shaft in cohesionless soil", *J. Geotech. Geoenviron. Eng.*, **132**(4), 478-487. https://doi.org/10.1061/(ASCE)1090-0241(2006)132:4(478).

Ni, J.C. and Cheng, W.C. (2010), "Monitoring and modeling grout efficiency of lifting structure in soft clay", *Int. J. Geomech.*, **10**(6), 223-229. https://doi.org/10.1061/(ASCE)GM.1943-5622.0000026.

Pellet, F. (2009), "Contact between a tunnel lining and a damage-susceptible viscoplastic medium", *Comput. Model. Eng. Sci.*, **52**(3), 279-295.

Sharifzadeh, M., Tarifard, A. and Moridi, M.A. (2013), "Time-dependent behavior of tunnel lining in weak rock mass based on displacement back analysis method", *Tunn. Undergr. Sp. Technol.*, **38**, 348-356. https://doi.org/10.1016/j.tust.2013.07.014.

Spagnoli, G., Scheller, P. and Doherty, P. (2016), "In situ and laboratory tests on a novel offshore mixed-in-place pile for oil and gas platforms", *J. Petrol. Sci. Eng.*, **145**, 502-509. https://doi.org/10.1016/j.petrol.2016.06.027.

Thiyyakkandi, S., McVay, M., Bloomquist, D. and Lai, P. (2012), "Measured and predicted response of a new jetted and grouted precast pile with membranes in cohesionless soils", *J. Geotech. Geoenviron. Eng.*, **139**(8), 1334-1345.

Thiyyakkandi, S., McVay, M., Bloomquist, D. and Lai, P. (2013), "Experimental study, numerical modeling of and axial prediction approach to base grouted drilled shafts in cohesionless soils", *Acta Geotechnica*, **9**(3), 439-454. https://doi:10.1007/s11440-013-0246-3.

Voottipruex, P., Bergado, D.T., Suksawat, T., Jamsawang, P. and Cheang, W. (2011), "Behavior and simulation of deep cement mixing (dcm) and stiffened deep cement mixing (sdcm) piles under full scale loading", *Soils Found.*, **51**(2), 307-320. https://doi.org/10.3208/sandf.51.307.

Wang, Z.B., Zou, J.F. and Yang, H. (2018), "A new approach for the fracture grouting pressure in soil mass", *Adv. Mech. Eng.*, **10**(7), 1687814018786435. https://doi.org/10.1177/1687814018786435.

Xia, Z.Q. and Zou, J.F. (2017), "Simplified approach for settlement analysis of vertically loaded pile", *J. Eng. Mech.*, **143**(11). 04017124. https://doi.org/10.1061/(ASCE)EM.1943-7889.0001334.

Zhang Q.Q., Li, S.C., Liang, F.Y., Yang, M. and Zhang, Q. (2014), "Simplified method for settlement prediction of single pile and pile group using a hyperbolic model", *Int. J. Civ. Eng.*, **12**(2), 179-192.

Zhang, Q.Q. and Zhang, Z.M. (2012), "Simplified calculation approach for settlement of single pile and pile groups", *J. Comput. Civ. Eng.*, **26**(6), 750-758. https://doi.org/10.1061/(ASCE)cp.1943-5487.0000167.

Zhou, J.J., Gong, X.N., Wang, K.H., Zhang, R. H. and Yan, J.J. (2017), "A simplified nonlinear calculation method to describe the settlement of pre-bored grouting planted nodular piles", *J. Zhejiang Univ. Sci. A*, **18**(11), 895-909. https://doi.org/10.1631/jzus.A1600640.

Zou, J.F., Yang, T., Wang, L., Guo, W.J. and Huang, F.L. (2019), "A numerical stepwise approach for cavity expansion problem in strain-softening rock or soil mass", *Geomech. Eng.*, **18**(3), 225-234. https://doi.org/10.12989/gae.2019.18.3.225.

CC